



This is a repository copy of *Analysis and design optimization of an improved axially magnetized tubular permanent-magnet machine* .

White Rose Research Online URL for this paper:
<http://eprints.whiterose.ac.uk/827/>

Article:

Wang, J.B., Howe, D. and Jewell, G.W. (2004) Analysis and design optimization of an improved axially magnetized tubular permanent-magnet machine. IEEE Transactions on Energy Conversion, 19 (2). pp. 289-295. ISSN 0885-8969

<https://doi.org/10.1109/TEC.2004.827026>

Reuse

Unless indicated otherwise, fulltext items are protected by copyright with all rights reserved. The copyright exception in section 29 of the Copyright, Designs and Patents Act 1988 allows the making of a single copy solely for the purpose of non-commercial research or private study within the limits of fair dealing. The publisher or other rights-holder may allow further reproduction and re-use of this version - refer to the White Rose Research Online record for this item. Where records identify the publisher as the copyright holder, users can verify any specific terms of use on the publisher's website.

Takedown

If you consider content in White Rose Research Online to be in breach of UK law, please notify us by emailing eprints@whiterose.ac.uk including the URL of the record and the reason for the withdrawal request.



eprints@whiterose.ac.uk
<https://eprints.whiterose.ac.uk/>

Analysis and Design Optimization of an Improved Axially Magnetized Tubular Permanent-Magnet Machine

Jiabin Wang, *Senior Member, IEEE*, David Howe, and Geraint W. Jewell

Abstract—This paper describes the analysis and design optimization of an improved axially magnetized tubular permanent-magnet machine. Compared with a conventional axially magnetized tubular machine, it has a higher specific force capability and requires less permanent-magnet material. The magnetic field distribution is established analytically in the cylindrical coordinate system, and the results are validated by finite-element analyses. The analytical field solution allows the analytical prediction of the thrust force and back-electromotive force (emf) in closed forms, which, in turn, facilitates the characterization of a machine, and provides a basis for design optimization and system dynamic modeling.

Index Terms—Linear motors, permanent-magnet motors, system analysis and design.

I. INTRODUCTION

THE DEMAND for linear electrical machines, for both controlled motion and electrical power generation, has increased steadily in recent years. For example, for applications in the high-speed packaging and manufacturing sectors, linear electromagnetic machines, which provide thrust force directly to a payload without the need to convert rotary to linear motion, offer significant advantages in terms of simplicity, efficiency, positioning accuracy, and dynamic performance—in both acceleration capability and bandwidth. Of the various types and configurations of linear motor, tubular permanent-magnet topologies are particularly attractive [1] since they have a high thrust force density and high efficiency, no end windings, and zero net attractive force between stator and armature. There are various tubular motor topologies [2], [3], in which the armature may be either air-cored or iron-cored. However, it has been shown [4] that an axially magnetized topology, Fig. 1, has a higher specific force capability than other candidate topologies, but requires more permanent-magnet material. This topology also has advantages with regard to the cost of manufacture, since axially anisotropic magnets are widely available, and they are magnetized simply by placing them in a solenoid impulse magnetizing fixture.

This paper describes the analysis and design of an improved axially magnetized tubular permanent-magnet machine, as shown in Fig. 2, in which both the magnets and the associated

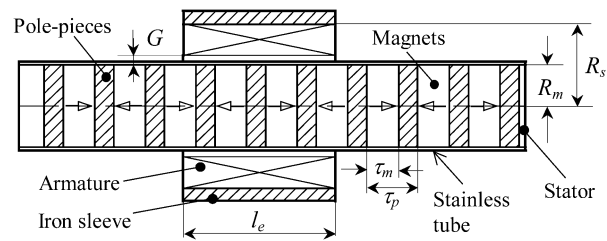


Fig. 1. Conventional axially magnetized tubular PM machine topology.

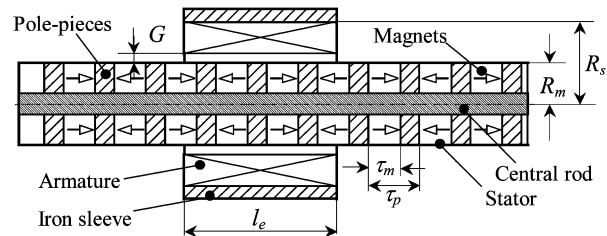


Fig. 2. Proposed machine topology.

pole-pieces are annular shaped and supported by a nonferromagnetic (stainless steel, for example) rod. It offers several advantages over the conventional topology shown in Fig. 1. First, it eliminates the need for a nonmagnetic tube to contain the magnets and pole-pieces, so that the effective magnetic air gap between the stator and armature is reduced. It also reduces the volume of permanent-magnet material. Although there will be some flux leakage via the central rod, the reduction in force capability can be relatively small. Furthermore, for moving-magnet machines, it can reduce the moving mass, and thereby increase the attainable acceleration. Further, in order to inhibit corrosion and/or to satisfy legislative standards, the surface of the magnets/pole-pieces can be covered with relatively thin protective coating.

In order to facilitate design optimization and accurate dynamic modeling, a variety of techniques has been employed to predict the magnetic field distribution in tubular permanent-magnet machines [2], the most common approach being to employ a lumped equivalent circuit [5], [6]. However, while this allows the relationship between critical design parameters and machine performance to be established analytically, it suffers from problems associated with model inaccuracy, particularly when flux leakage is significant and the flux paths are complex. Therefore, numerical analysis of the field distribution and evaluation of performance [7]–[9] are also employed. However,

Manuscript received December 16, 2002.

The authors are with the Department of Electronic and Electrical Engineering, the University of Sheffield, Sheffield S1 3JD, U.K. (e-mail: j.b.wang@sheffield.ac.uk).

Digital Object Identifier 10.1109/TEC.2004.827026

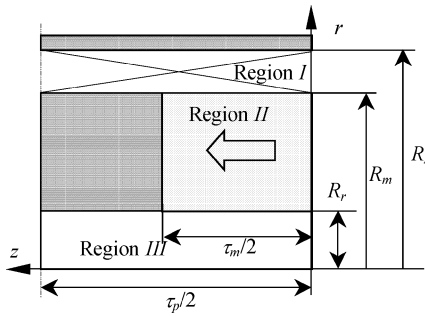


Fig. 3. Field regions.

while techniques such as finite-element analysis provide an accurate means of determining the field distribution, with due account of saturation, etc., they remain time consuming and do not provide as much insight as analytical solutions into the influence of the design parameters on the machine behavior. To overcome the aforementioned problems, an analytical solution for the magnetic field distribution has been established in the cylindrical coordinate system [3]. It is an extension to the analysis which has been developed for tubular permanent-magnet machines to account specifically for the topology in Fig. 2 [10]. The analytical solution allows the prediction of the thrust force and the back-electromotive force (emf) in closed forms, which, in turn, facilitates the characterization of machines and provides a basis for design optimization and system dynamic modeling.

II. FIELD DISTRIBUTION DUE TO PERMANENT MAGNET SOURCE

A. Magnetic Field Distribution

In order to establish an analytical solution for the magnetic field distribution, the following assumptions are made.

- i) The axial length of the machine is infinite so that the field distribution is axially symmetric and periodic in the z -direction.
- ii) The armature is slotless and the permeability of the iron is infinite.

However, the effect of slotting, if present, can be taken into account by introducing a Carter coefficient. Consequently, the magnetic field analysis is confined to three regions, viz. the airspace/winding regions *I* and *III*, and the permanent-magnet region *II*, as shown in Fig. 3, for which the field equations, in terms of the magnetic vector potential A_θ are governed by

$$\begin{cases} \frac{\partial}{\partial z} \left(\frac{1}{r} \frac{\partial}{\partial z} (r A_{I,III\theta}) \right) + \frac{\partial}{\partial r} \left(\frac{1}{r} \frac{\partial}{\partial r} (r A_{I,III\theta}) \right) = 0 \\ \frac{\partial}{\partial z} \left(\frac{1}{r} \frac{\partial}{\partial z} (r A_{II\theta}) \right) + \frac{\partial}{\partial r} \left(\frac{1}{r} \frac{\partial}{\partial r} (r A_{II\theta}) \right) = -\mu_0 \nabla \times \mathbf{M}. \end{cases} \quad (1)$$

\mathbf{M} is the magnetization vector of the magnets and is given by

$$\mathbf{M} = M_z e_z \quad (2)$$

TABLE I
DESIGN PARAMETERS OF TUBULAR PM MACHINE (M)

R_s	R_m	R_r	τ_p	τ_m
0.03	0.0243	0.005	0.0282	0.0197

where M_z denotes the component of \mathbf{M} in the z direction and may be expressed as the Fourier series

$$M_z = \sum_{n=1,2,\dots} \frac{4B_{rem}}{\mu_0 \pi (2n-1)} \sin \left(\frac{(2n-1)\pi \tau_m}{2\tau_p} \right) \cos m_n z \quad (3)$$

where τ_m is the axial length of the magnets, τ_p is the pole-pitch, and $m_n = (2n-1)\pi/\tau_p$. The boundary conditions to be satisfied by the solution to (1) are

$$\begin{aligned} B_{Iz}|_{r=R_s} &= 0 & B_{IIIr}|_{r=0} &= 0 \\ B_{zI}|_{z=\tau_p/2} &= 0 & B_{rI}|_{z=0} &= 0 \\ B_{Iz}|_{\substack{r=R_m \\ \tau_m/2 < z < \tau_p/2}} &= 0 & B_{IIIz}|_{\substack{r=R_r \\ \tau_m/2 < z < \tau_p/2}} &= 0 \\ B_{IIr}|_{z=\tau_m/2} &= 0 \\ B_{Ir}|_{\substack{r=R_m \\ 0 \leq z \leq \tau_m/2}} &= B_{IIr}|_{\substack{r=R_m \\ 0 \leq z \leq \tau_m/2}} \\ H_{Iz}|_{\substack{r=R_m \\ 0 \leq z \leq \tau_m/2}} &= H_{IIz}|_{\substack{r=R_m \\ 0 \leq z \leq \tau_m/2}} \\ B_{IIr}|_{\substack{r=R_r \\ 0 \leq z \leq \tau_m/2}} &= B_{IIIr}|_{\substack{r=R_r \\ 0 \leq z \leq \tau_m/2}} \\ H_{IIz}|_{\substack{r=R_r \\ 0 \leq z \leq \tau_m/2}} &= H_{IIIz}|_{\substack{r=R_r \\ 0 \leq z \leq \tau_m/2}} \end{aligned}$$

$$\int_{R_r}^{R_m} r B_{IIz}(r, \tau_m/2) dr = \int_{\tau_m/2}^{\tau_p/2} [R_m B_{Ir}(R_m, z) - R_r B_{IIIr}(R_r, z)] dz. \quad (4)$$

Solving (1) subject to the boundary conditions of (4) yields

$$\begin{aligned} B_{Ir} &= \sum_{n=1}^{\infty} [a_{In} B_{I1}(m_n r) + b_{In} B_{K1}(m_n r)] \sin m_n z \\ B_{Iz} &= \sum_{n=1}^{\infty} [a_{In} B_{I0}(m_n r) - b_{In} B_{K0}(m_n r)] \cos m_n z \end{aligned} \quad (5-a)$$

$$\begin{aligned} B_{IIr} &= \sum_{j=1}^{\infty} [a_{IIj} B_{I1}(q_j r) + b_{IIj} B_{K1}(q_j r)] \sin q_j z \\ B_{IIz} &= \sum_{j=1}^{\infty} [a_{IIj} B_{I0}(q_j r) - b_{IIj} B_{K0}(q_j r)] \cos q_j z + B_0 \end{aligned} \quad (5-b)$$

$$\begin{aligned} B_{IIIr} &= \sum_{n=1}^{\infty} a_{III n} B_{I1}(m_n r) \sin m_n z \\ B_{IIIz} &= \sum_{n=1}^{\infty} a_{III n} B_{I0}(m_n r) \cos m_n z \end{aligned} \quad (5-c)$$

where $B_{I0}(\bullet)$ and $B_{I1}(\bullet)$ are modified Bessel functions of the first kind; $B_{K0}(\bullet)$ and $B_{K1}(\bullet)$ are modified Bessel func-

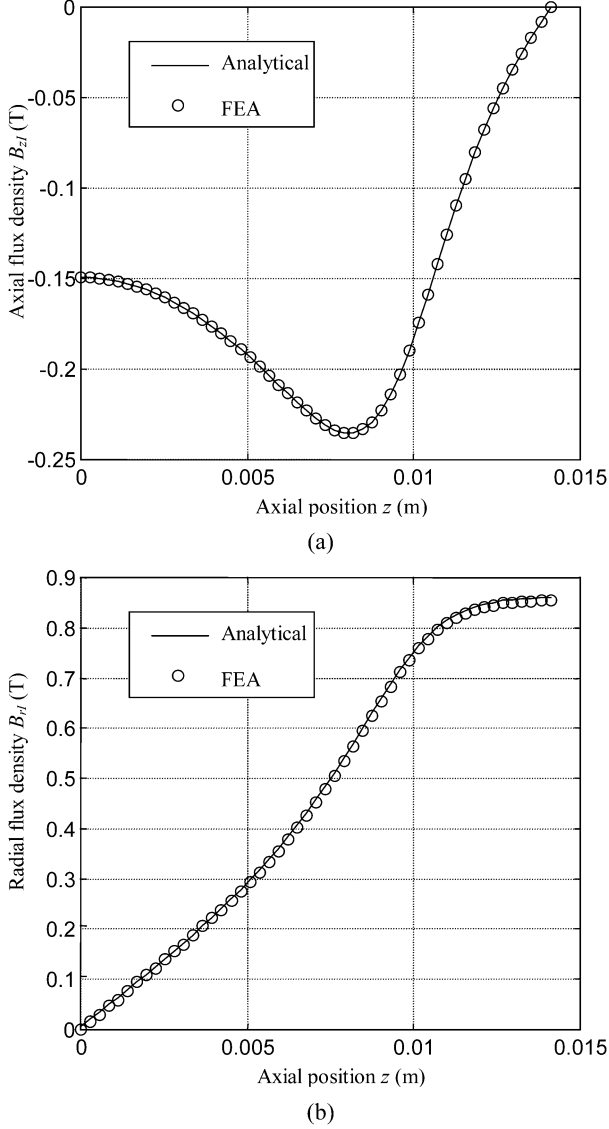


Fig. 4. Comparison of axial and radial flux density components as functions of axial position z at $r = (R_m + R_s)$ (a) axial flux density B_{zI} , (b) radial flux density B_{rI} .

tions of the second kind, of order 0 and 1, respectively; $q_j = 2\pi j/\tau_m$ and a_{In} , b_{In} , a_{IIj} , b_{IIj} , $a_{III n}$, and B_0 are defined in the Appendix.

B. Comparison With Finite-Element Calculations

The main design parameters of the tubular machine, for which the analytical field solution has been obtained, are given in Table I. The magnets are sintered NdFeB, with $B_{rem} = 1.15$ T. The analytical field distribution has been validated by finite-element calculation of the radial and axial variations of the radial and axial flux density components in the airgap/winding regions.

The finite-element solution was obtained by applying a periodic boundary condition at the axial boundaries $z = \pm\tau_p$ and imposing the natural Neumann boundary condition at the surface of the armature sleeve. Fig. 4 compares numerically and analytically calculated distributions of the axial and radial flux

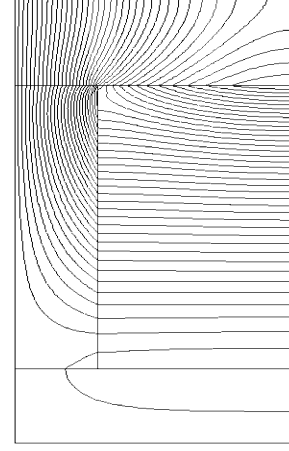


Fig. 5. Open-circuit flux distribution.

density components B_{zI} and B_{rI} as functions of the axial position z at a constant radius $r = 0.0261$. It will be seen that the analytical solution agrees extremely well with the finite-element prediction.

Fig. 5 shows the finite-element (FE) predicted flux distribution in the tubular machine. As can be seen, flux leakage via the nonmagnetic rod is very small, and has a negligible effect on the winding flux linkage.

III. EMF AND FORCE PREDICTION

It has been shown in [3] that the flux linkage of a phase winding, comprising a number of series connected coils each displaced by a winding pitch τ_{wp} is given by

$$\Psi_{wp} = \sum \Phi_{wn} \sin m_n \left(\frac{z - \tau_{wp}}{2} \right) \quad (6)$$

where

$$\Phi_{wn} = \frac{-4\pi N_{wp} K_{rn} K_{dnpn}}{(R_s - R_i) m_n} \quad (7)$$

where N_{wp} is the number of series turns per phase, and R_i is the inner radius of the winding. K_{dnpn} is defined as the winding factor of the $(2n - 1)$ th harmonic and is given by

$$K_{dnpn} = \frac{\sin \left(\frac{m_n \tau_w}{2} \right)}{\left(\frac{m_n \tau_w}{2} \right)} * \sin \left(\frac{m_n \tau_{wp}}{2} \right) \quad (8)$$

and K_{rn} is the coefficient related to the $(2n - 1)$ th harmonic in the radial field distribution and is given by

$$K_{rn} = \int_{R_i}^{R_s} r [a_{In} B I_1(m_n r) + b_{In} B K_1(m_n r)] dr. \quad (9)$$

Hence, the induced emf per phase is obtained as

$$e_{wp} = \frac{-d\Psi_{wp}}{dt} = -v \sum \Phi_{wn} m_n \cos m_n \left(\frac{z - \tau_{wp}}{2} \right) \quad (10)$$

where v is the velocity of the armature. Fig. 6 compares the numerically and analytically predicted flux linkage of one

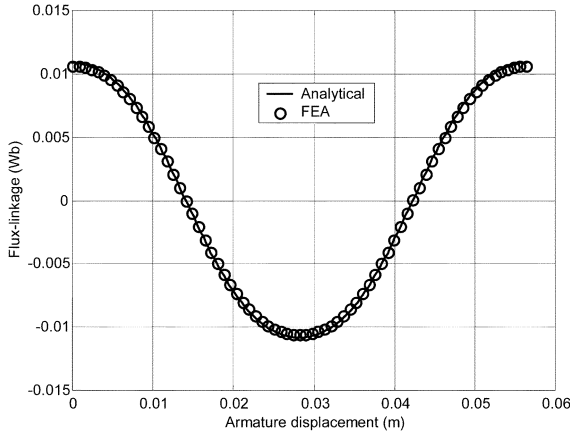


Fig. 6. Comparison of flux linkage per phase per pole as a function of axial displacement of the armature.

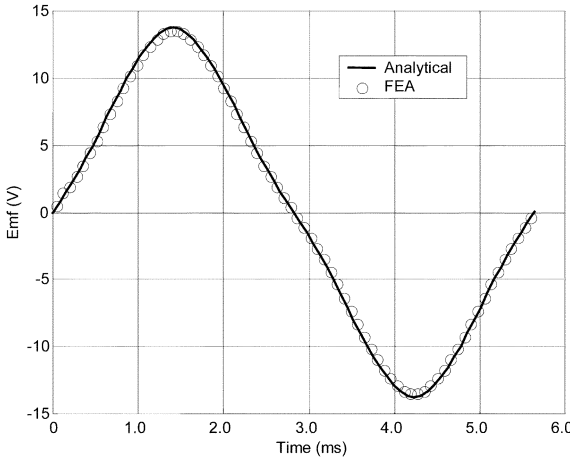


Fig. 7. Comparison of emf per phase per pole as a function of time at an armature speed of 10 (m/s).

pole-pair phase winding with $N_{wp} = 10$, while Fig. 7 compares the corresponding emf waveforms at an armature velocity of 10 (m/s) for the same machine parameters given in Table I. Again, an excellent agreement is observed.

Similarly, the axial force exerted on a phase winding, comprising coils spanning a number of pole-pairs p and having a current density J , is given by

$$F_{wp} = \sum J K_n \cos m_n \left(\frac{z - \tau_{wp}}{2} \right) \quad (11)$$

$$K_n = -4\pi p \tau_w K_{rn} K_{dpn}$$

where τ_w is the axial width of the phase winding per pole. With balanced sinusoidal three-phase currents, it can be shown [4] that the total thrust force is given by

$$F = F_1 + \sum_{\substack{n=3k+1 \\ k=1,2,\dots}}^{\infty} F_{n1} \cos \left[(2n-2) \left(\frac{\pi z}{\tau_p} \right) \right] \\ + \sum_{\substack{n=3k+3 \\ k=0,1,2,\dots}}^{\infty} F_{n3} \cos \left[(2n-5) \left(\frac{\pi z}{\tau_p} \right) \right] \quad (12)$$

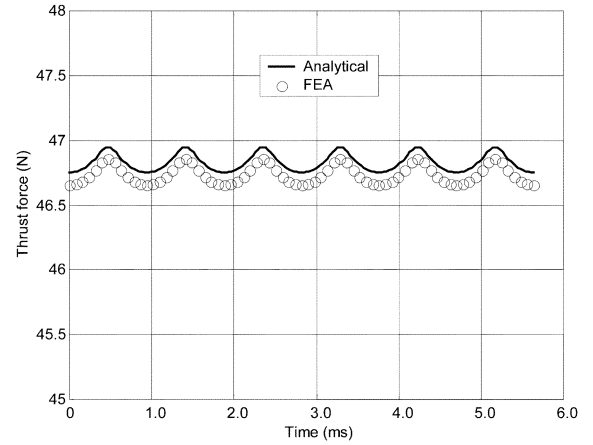


Fig. 8. Comparison of thrust force waveforms per phase per pole at an armature speed of 10 m/s under sinusoidal excitation.

where F_1 , F_{n1} , and F_{n3} are given by

$$F_1 = 12\sqrt{2}p\tau_p K_{r1} J_{rms} \sin \left(\frac{\pi}{6} \right) \\ F_{n1} = \sqrt{2}J_{rms} \left(\frac{3}{2} \right) K_n (-1)^k \\ n = 3k + 1, \quad k = 1, 2, \dots \\ F_{n3} = \sqrt{2}J_{rms} \left(\frac{3}{2} \right) K_n (-1)^{k+1} \\ n = 3k + 3, \quad k = 0, 1, 2, \dots \quad (13)$$

and J_{rms} is the root mean square (rms) current density. As will be evident from (13), the force ripple due to triplen harmonics in the radial field distribution is zero. The normalized total force ripple is, therefore, given by

$$\text{TFR} = \frac{\sqrt{\sum_{n=3} F_n^2}}{F_1} \\ = \frac{\sqrt{\sum_{n=3} K_n^2}}{K_1}, \quad n \neq 3k + 2, \quad k = 0, 1, 2, \dots \quad (14)$$

Fig. 8 shows the comparison of thrust force waveforms, predicted by both FE and the analytical solution, at an armature speed of 10 m/s for the same machine parameters given in Table I. In both predictions, the armature is supplied with a three-phase sinusoidal current having an amplitude of 25 (A). It should be noted that the thrust forces in Fig. 8 do not include the cogging force component due to finite armature length as a periodic condition is applied in both analytical and FE models.

IV. DESIGN OPTIMIZATION

Having established an analytical expression for the force capability, the design of the tubular machine can be optimized with respect to a given criterion, for example, for maximum force capability or for minimum cost for a given performance specification and volumetric constraint. In this paper, design optimization is addressed at maximizing the force capability, subject to satisfying other performance specifications.

It has been shown [4] that the permissible winding copper loss and iron loss are governed by the dissipation capability of the machine, that is

$$\pi l_e (R_s^2 - R_i^2) k_{pf} \rho J_{\text{rms}}^2 + p_{fe} = k_\theta A \Delta T \quad (15)$$

where k_{pf} is the winding packing factor, ρ is the resistivity of copper, k_θ is the armature surface temperature coefficient, A is the armature surface dissipation area, and ΔT is the allowable temperature rise of the windings. The iron loss p_{fe} can be predicted using the formula in [11] from the flux density derived from the analytical field solution. The permissible current density is, therefore, given by

$$J_{\text{rms}} = \sqrt{\frac{k_\theta A \Delta T - p_{fe}}{\pi l_e (R_s^2 - R_i^2) k_{pf} \rho}}. \quad (16)$$

Thus, (13) and (16) relate the force capability to the design parameters under a given thermal condition.

The analytical field solution is obtained assuming that the armature and stator iron pole-pieces are infinitely permeable. Although saturation of the cores is unlikely in slotless permanent-magnet (PM) machines, it is prudent to account for saturation during the design optimization process when different combinations of design parameters are being considered. Thus, a fictitious radial air gap is introduced between the armature windings and the outer armature sleeve to account for core saturation, its effectiveness being confirmed by finite-element analysis [4].

The main design parameters that influence the performance of the machine are shown in Fig. 2, where l_e is the active armature length, G is the air-gap length, and R_e is the outer radius of the armature. For slotless machines, it has been shown that the influence of end effects associated with the finite armature length on the flux linkage and thrust force of the windings are negligible [12]. Hence, (12)–(14) and (16) can be used to predict the force capability and the force ripple. In order that the findings are independent of machine size, the thrust force due to the fundamental component of the radial magnetic field is divided by the volume of the armature $\pi R_e^2 l_e$ to give the force density. Thus, the design objective is to optimize the machine parameters so as to maximize the force density and minimize the total force ripple, while satisfying other given specifications.

For a given outer radius R_s , the design parameters that affect the force density and the force ripple are τ_m/τ_p , R_m/R_s , τ_p/R_s , and G . However, for slotless machines, the influence of the air-gap length is not as significant as for slotted machines and in this study, it is, therefore, considered to be constant. It has been shown [4] that the influence of the ratio of τ_m/τ_p on the performance is largely independent of the other two-dimensional ratios. By way of example, Fig. 9 shows the variation of the force density and the normalized total force ripple with τ_m/τ_p and R_m/R_s , assuming $B_{rem} = 1.15$ (T), $\mu_r = 1.05$, $\rho = 1.71 \times 10^{-7}$ ($\Omega\cdot\text{m}$), $k_{pf} = 0.5$, $k_\theta = 4.3$ (W/m 2 °C), $\Delta T = 100$ (°C), $R_s = 0.03$ (m), $\tau_p/R_s = 0.94$, $G = 0.001$ m, and $R_e = 0.030$ m.

As can be seen, the variation of the force density with τ_m/τ_p is essentially similar irrespective of the ratio of R_m/R_s . The general trend is that an increase in τ_m/τ_p results in an increase in the force capability. However, the rate of increase of the force

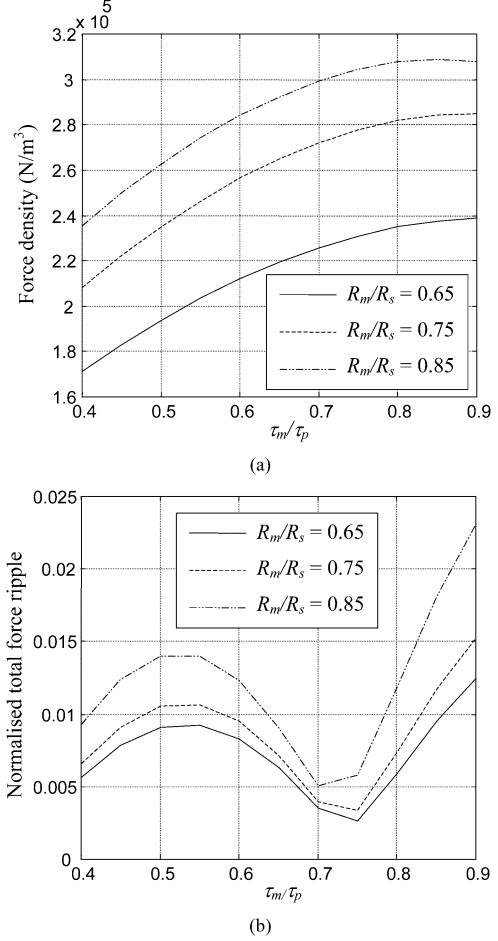


Fig. 9. Variation of force density and force ripple as functions of τ_m/τ_p (a) force density and (b) normalized force ripple.

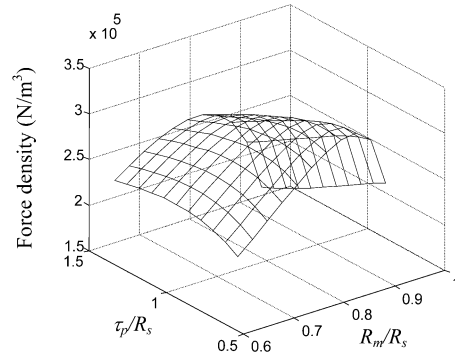


Fig. 10. Variation of force density as functions of R_m/R_s and τ_p/R_s , $\tau_m/\tau_p = 0.70$.

capability reduces progressively as τ_m/τ_p approaches 0.9. The higher the ratio of τ_m/τ_p , the greater the magnet volume and, therefore, the more expensive the machine. With regard to the total force ripple, this exhibits a local maximum at $\tau_m/\tau_p \approx 0.525$ and a minimum at $\tau_m/\tau_p \approx 0.725$. Thus, a value of τ_m/τ_p between 0.6 and 0.75 probably represents the best compromise between performance and magnet cost.

Fig. 10 shows the variation of the force density with R_m/R_s and τ_p/R_s from which it is evident that for a given value of τ_p/R_s , there is an optimal ratio of R_m/R_s which results in the maximum force density. For a given value of R_m/R_s , there is

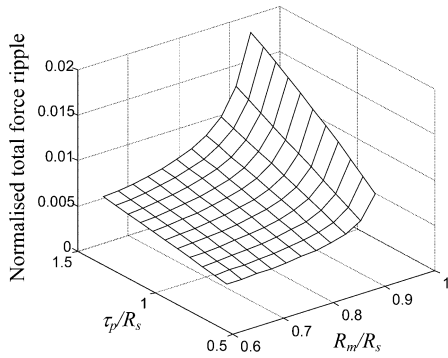


Fig. 11. Variation of normalized force ripple as functions of R_m/R_s and τ_p/R_s , $\tau_m/\tau_p = 0.70$.

also an optimal value for τ_p/R_s , which results in the maximum force density.

The optimal combination of dimensional ratios for R_m/R_s and τ_p/R_s for this particular example are 0.85 and 0.7, respectively, which results in a maximum force density of $3.02 \times 10^5 \text{ N/m}^3$.

Fig. 11 shows the variation of the total force ripple as a function of R_m/R_s and τ_p/R_s . As will be seen, the force ripple increases when both of these dimensional ratios are increased. However, at the optimal dimensional ratios for maximum force density, the normalized total force ripple is less than 0.3%.

V. COMPARISON WITH THE CONVENTIONAL MACHINE TOPOLOGY

In order to compare its performance with that of a conventional machine topology (Fig. 1), both machines are assumed to be slotless, and they are designed to the same criterion and with the same thermal constraint with due account of core saturation. Fig. 12 compares the force density and the normalized force ripple of the two machines as a function of τ_m/τ_p , assuming $R_s = 0.03 \text{ m}$, $B_{rem} = 1.15 \text{ T}$, and an air-gap length of 0.001 m , with $R_m/R_s = 0.8$ and $\tau_p/R_s = 0.94$, which are optimal ratios for the conventional machine topology [4]. The wall thickness of the nonmagnetic containment sleeve in the conventional motor is assumed to be 0.001 (m) . Thus, it has an effective air gap of 0.002 m . In the proposed machine topology, the inner radius of the magnets/pole-pieces is 0.005 m .

As will be seen, in this particular case, the force density of the proposed tubular machine topology is $\sim 12.5\%$ higher than that of the conventional machine despite the fact that it requires 4.3% less permanent-magnet material. This is due to the smaller air gap, which results in a slightly larger winding area and a more radially orientated field distribution over the cross-section of the winding. Its normalized force ripple is, however, slightly higher although with $\tau_m/\tau_p \approx 0.725$, the force ripple of both machines is below 0.2% , which is likely to be negligible compared with the cogging force which results from end effects.

It should be noted that for machines with a slotted armature, the proposed topology will be even more beneficial than the conventional counterpart as the absence of the containment tube can significantly reduce the magnetic air gap and, hence, results in a greater increase in force density.

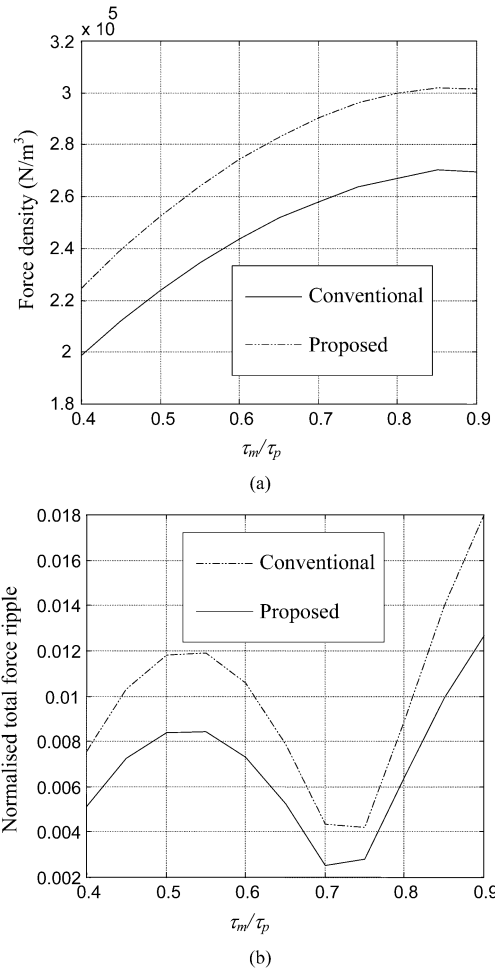


Fig. 12. Comparison of force density and normalized force ripple. (a) Force density. (b) Normalized force ripple.

VI. CONCLUSION

A modified design of axially magnetized tubular permanent-magnet machine has been proposed, and its magnetic field distribution has been analytically established. This allows its force capability and force ripple to be expressed as functions of various dimensional ratios, which provides a useful tool for assessing the influence of leading design parameters on the machine performance and for making comparative studies. It has been shown that the proposed machine design has a higher force capability than that of a conventional machine, while it requires less permanent-magnet material. It should be noted, however, that the design needs to be appraised mechanically in regards to the stiffness of the thrust rod and economically in regards to the machining of the inner bore of the magnets and pole pieces for example.

APPENDIX

Definition of a_{in} , b_{in} , a_{IIj} , b_{IIj} , a_{III_n} , and B_0 . Let

$$\begin{aligned}
 c_{1n} &= BI_0(m_n R_s) & c_{2n} &= BK_0(m_n R_s) \\
 c_{3n} &= BI_1(m_n R_r) & c_{4n} &= BI_0(m_n R_r) \\
 c_{5n} &= BI_0(m_n R_m) & c_{6n} &= BK_0(m_n R_m) \\
 c_{7n} &= BI_1(m_n R_m) & c_{8n} &= BK_1(m_n R_m) \\
 c_{1j} &= BI_1(q_j R_m) & c_{2j} &= BK_1(q_j R_m)
 \end{aligned}$$

$$\begin{aligned}
c_{3j} &= BI_0(q_j R_m) & c_{4j} &= BK_0(q_j R_m) \\
c_{5j} &= BI_1(q_j R_r) & c_{6j} &= BK_1(q_j R_r) \\
c_{7j} &= BI_0(q_j R_r) & c_{8j} &= BK_0(q_j R_r) \\
d_{1n} &= \frac{c_{2n} c_{7n}}{c_{1n}} + c_{8n} & d_{2n} &= \frac{c_{5n} c_{2n}}{c_{1n} - c_{6n}} \\
d_{1j} &= \frac{c_{4j} c_{6j}}{c_{2j}} & d_{2j} &= \frac{c_{8j} c_{6j}}{c_{2j}} \\
E_j &= \frac{\cos\left(\frac{q_j \tau_m}{2}\right) (c_{1j} R_m - c_{5j} R_r)}{q_j} \\
G_j &= \frac{\cos\left(\frac{q_j \tau_m}{2}\right) (c_{2j} R_m - c_{6j} R_r)}{q_j} \\
E_n &= \frac{d_{1n} R_m \cos\left(\frac{m_n \tau_m}{2}\right)}{m_n} \\
G_n &= \frac{R_r c_{3n} \cos\left(\frac{m_n \tau_m}{2}\right)}{m_n} & Q_n &= \frac{4 \sin\left[\frac{(2n-1)\pi \tau_m}{2\tau_p}\right]}{[\pi \mu_r (2n-1)]} \\
R_0 &= \frac{(R_m^2 - R_r^2)}{2} & B_n &= B_{rem} Q_n \\
v &= \frac{(m_n - q_j) \tau_m}{2} & u &= \frac{(m_n + q_j) \tau_m}{2} \\
F_{jn} &= \frac{\frac{\sin v}{v} - \frac{\sin u}{u}}{\mu_r \tau_p} \\
F_{nj} &= \frac{\left(\frac{\sin v}{v} + \frac{\sin u}{u}\right) \tau_m}{\mu_r \tau_p}.
\end{aligned}$$

Then, a_{IIj} , b_{IIj} , b_{In} , $a_{III n}$, and B_0 are solutions of the following $(2N_E + 2I_E + 1) \times (2N_E + 2I_E + 1)$ linear equations:

$$\begin{aligned}
c_{1j} a_{IIj} + c_{2j} b_{IIj} - \sum_n d_{1n} F_{jn} b_{In} &= 0 \\
c_{5j} a_{IIj} + c_{6j} b_{IIj} - \sum_n c_{3n} F_{jn} a_{III n} &= 0 \\
- \sum_j c_{3j} F_{nj} a_{IIj} + \sum_j d_{1j} F_{nj} b_{IIj} + d_{2n} b_{In} & \\
- Q_n B_0 &= -B_n \\
- \sum_j c_{7j} F_{nj} a_{IIj} + \sum_j d_{2j} F_{nj} b_{IIj} + c_{4n} a_{III n} & \\
- Q_n B_0 &= -B_n \\
\sum_j E_j a_{IIj} + \sum_j G_j b_{IIj} - \sum_n E_n b_{In} + \sum_n G_n a_{III n} & \\
+ R_0 B_0 &= 0
\end{aligned}$$

and $a_{in} = b_{in} c_{2n} / c_{1n}$, where N_E , I_E are the numbers of the harmonic terms used for the calculation of the flux density in regions I, III, and II, respectively.

REFERENCES

- [1] J. F. Eastham, "Novel synchronous machines: Linear and disc," *Proc. Inst. Elect. Eng., Elect. Power Appl.*, vol. 137, no. 1, pp. 49–58, 1990.
- [2] I. Boldea and S. A. Nasar, *Linear Electric Actuators and Generators*. Cambridge, U.K.: Cambridge Univ. Press, 1997.
- [3] J. Wang, G. W. Jewell, and D. Howe, "A general framework for the analysis and design of tubular linear permanent magnet machines," *IEEE Trans. Magn.*, vol. 35, pp. 1986–2000, May 1999.
- [4] —, "Design optimization and comparison of tubular permanent magnet machines," *Proc. Inst. Elect. Eng., Elect. Power Appl.*, vol. 148, no. 5, pp. 456–463, 2001.
- [5] R. E. Clark, D. S. Smith, P. H. Mellor, and D. Howe, "Design optimization of moving-magnet actuators for reciprocating electro-mechanical systems," *IEEE Trans. Magn.*, vol. 31, pp. 3746–3748, Nov. 1995.

- [6] T. Mizuno and H. Yamada, "Magnetic circuit analysis of a linear synchronous motor with permanent magnets," *IEEE Trans. Magn.*, vol. 28, pp. 3027–3029, Sept. 1992.
- [7] R. Akmes and J. F. Eastham, "Dynamic performance of a brushless DC tubular drive system," *IEEE Trans. Magn.*, vol. 25, pp. 3269–3271, Sept. 1989.
- [8] A. Basak and G. H. Shirkoobi, "Computation of magnetic field in D.C. brushless linear motors built with NdFeB magnets," *IEEE Trans. Magn.*, vol. 26, pp. 948–951, Mar. 1990.
- [9] J. F. Eastham, R. Akmes, and H. C. Lai, "Optimum design of brushless tubular linear machines," *IEEE Trans. Magn.*, vol. 26, pp. 2547–2549, Sept. 1990.
- [10] J. Wang, D. Howe, and G. W. Jewell, "An improved axially magnetised tubular permanent magnet machine," in *Proc. Int. Conf. Power Electron.*, Bath, U.K., 2002, pp. 303–308.
- [11] K. Atallah, Z. Q. Zhu, and D. Howe, "The prediction of iron losses in brushless permanent magnet dc motors," in *Proc. Int. Conf. Elect. Mach.*, 1992, pp. 814–818.
- [12] J. Wang, D. Howe, and G. W. Jewell, "Analytical prediction of fringing effect in tubular permanent magnet machines," in *Proc. Int. Symp. Linear Drives Ind. Applicat.*, 2001, pp. 304–309.



Jiabin Wang (SM'03) was born in Jiangsu Province, China, in 1958. He received the B.Eng. and M.Eng. degrees in electrical and electronic engineering from Jiangsu University of Science and Technology, Zhengjiang, China, in 1982 and 1986, respectively, and the Ph.D. degree in electrical and electronic engineering from the University of East London, London, U.K., in 1996.

Currently, he is a Senior Lecturer at the University of Sheffield, Sheffield, U.K. From 1986 to 1991, he was with the Department of Electrical Engineering at Jiangsu University of Science and Technology, where he was appointed a Lecturer in 1987 and an Associated Professor in 1990. He was a Postdoctoral Research Associate at the University of Sheffield, Sheffield, U.K., from 1996 to 1997, and a Senior Lecturer at the University of East London from 1998 to 2001. His research interests range from motion control to electromagnetic devices and their associated drives.



David Howe received the B.Tech. and M.Sc. degrees in electrical power engineering from the University of Bradford, Bradford, U.K., in 1966 and 1967, respectively, and the Ph.D. degree in electrical power engineering from the University of Southampton, Southampton, U.K.

Currently, he is a Professor of Electrical Engineering at the University of Sheffield, Sheffield, U.K., where he heads the Electrical Machines and Drives Research Group. He has held academic posts at Brunel University, London, U.K., and Southampton University, and spent a period in industry with NEI Parsons Ltd., Newcastle-Upon-Tyne, U.K., working on electromagnetic problems related to turbogenerators. His research activities span all facets of controlled electrical drive systems with particular emphasis on permanent-magnet-excited machines.

Dr. Howe is a Fellow of the Institution of Electrical Engineers, U.K.



Geraint W. Jewell was born in Neath, Wales, U.K., in 1966. He received the B.Eng. and Ph.D. degrees from the Department of Electronic and Electrical Engineering at the University of Sheffield, Sheffield, U.K., in 1988 and 1992, respectively.

Currently, he holds an Engineering and Physical Sciences Research Council Advanced Research Fellowship. From 1994 to 2000, he was a Lecturer in Electrical Machines and Drives Research Group, University of Sheffield. His research interests cover many aspects of both permanent-magnet and reluctance-based electrical machines and actuators.